Acta Cryst. (1986). B42, 152-159

Some New σ-Related Structures Determined by High-Resolution Electron Microscopy

BY D. X. LI AND K. H. KUO

Institute of Metal Research, Academia Sinica, 110015 *Shenyang, People's Republic of China*

(*Received* 7 *January* 1985; *accepted* 7 *June* 1985)

Abstract

Some new tetrahedrally close-packed metallic phases, called *F*, *K* and *J*, have been found in a Ni-based superalloy and their structures determined by high-resolution electron microscopy (HREM) and electron diffraction: *F*: *P6/mmm*, $a = b = 12{\cdot}5$, $c = 4{\cdot}5$ Å, $Z = 52$; *K*: *Pmmm*, $a = 12{\cdot}5$, $b = 17{\cdot}1$, $c = 4{\cdot}5$ Å, $Z = 82$; *J*: *Pmmm*, $a = 4{\cdot}5$, $b = 12{\cdot}5$, $c = 4{\cdot}5$ Å, $Z = 22$ (e.s.d.'s of lattice parameters *ca* 0·05 Å). Like $\sigma(3^2434)$ and $H(3^34^2)$ phases, they are also composed of hexagonal antiprisms but in different juxtaposing configurations: 3^6+3^2434 (1:6), 3^6+3^2434 (1:10) and $3^6+3^34^2$ (1:2), respectively, for *F*, *K* and *J* phases.

1. Introduction

Some of the tetrahedrally close-packed structures of intermetallic phases of transition metals, which contain only interpenetrating coordination polyhedra with CN12, 14 or 15, are in most cases generated by the juxtaposing of hexagonal antiprisms. For example, the celebrated σ phase has a 3^2434 tessellation of these hexagonal antiprisms. Owing to various possibilities of the juxtaposing of hexagonal antiprisms, a number of new phases can be formed. Frank & Kasper (1959) first predicted a series of hypothetical structures in which the hexagonal antiprisms form 3^34^2 or 3^6+3^2434 (1:6) tessellations. In previous work (Ye & Kuo, 1984; Ye, Li & Kuo, 1984) the crystal structure of the former in Fe- and Ni-based superalloys, called *H*, was determined by structure imaging in combination with electron diffraction analysis and its space group was found to be *Cmmm*, with $a = 4{\cdot}5$, $b = 17{\cdot}5$, $c = 4{\cdot}5$ Å. Some new σ-related phases have now been found by HREM in a Ni-based superalloy, and one of them is identical to the hypothetical structure suggested by Frank & Kasper (1959) with a 3^6+3^2434 (1:6) network of hexagonal antiprisms. A similar structure with a 3^6+3^2434 (1:10) network has also been found. They are called *F* and *K* phases, respectively, in honor of Frank & Kasper. A third structure with the $3^6+3^34^2$ (1:2) tessellation of hexagonal antiprisms is called the *J* phase. In the high-resolution image, taken under favorable imaging conditions as described in § 2, the hexagonal antiprisms are imaged as bright spots and the networks of 3^2434, 3^6+3^2434 (1:6), 3^6+3^2434 (1:10) and $3^6+3^34^2$ (1:2) can be clearly seen. These demonstrate clearly the structural characteristics of the σ, *F*, *K* and *J* phases. Because of the smallness of these new phases, their structure determinations have to rely upon HREM, computer simulation and selected-area electron diffraction. Fortunately, this is greatly facilitated by the close relationship between these new structures and the σ phase, all being made up of square Zr_4Al_3 and triangular Cr_3Si elementary blocks in different combinations. In this paper the crystal structures of the *F*, *K* and *J* phases and their relationship to σ are presented. The domain structures of these new phases and some hypothetical structures predicted from the high-resolution images will also be briefly discussed.

It is very gratifying indeed to be informed that the structure of the *F* phase has been independently and simultaneously determined by Lin & Steeds (1986) of Bristol University by means of another novel technique - convergent-beam electron diffraction, as presented in the following paper. A unit of this *F* structure has also been noted before (see Fig. 15 of Ye & Kuo, 1984).

2. Structure determination

These new phases were found in a Ni-based superalloy with the following composition (in wt%) after heating at 1323 K for 2 h:

C	Cr	W	Mo	Al	Ti	B
<0·05	20	8·0	8·0	0·6	0·6	0·005

Ce	Zr	Si	Mn	Fe	Ni
0·05	0·06	<0·8	<0·5	<2·0	balance.

These new phases were extracted electrolytically from this alloy in an electrolyte consisting of 4% HCl and 8% grease in methyl alcohol at 270-283 K with a current density of 40 to 60 mA cm^{-2}.

In most cases the *F* phase can be separated alone and its chemical composition has been determined directly in a Hitachi H-700H electron microscope by means of X-ray energy-dispersive analysis with an EDAX 9100 system. The result of the quantitative X-ray analysis (at.%) of the *F* phase is:

Mo	W	Ni	Cr
45·1	11·3	19·9	23·7.

0108-7681/86/020152-08$01.50

High-resolution images were taken in a JEM 200CX electron microscope equipped with a top-entry stage, C_s of the pole pieces being 1·2 mm with a point resolution of 2·6 Å. The objective aperture size used corresponded to a radius of 0·55 $Å^{-1}$ in reciprocal space.

The computer image simulation was carried out using the multislice program written by Ishizuka (1982) including first- and second-order partial coherent envelopes. Our image simulation has shown that the images changed rapidly with thickness and also with defocus value, so that careful image matching is necessary to ascertain the best imaging conditions. The parameters used in the image simulation are given in Table 1. The images were computed for a range of thickness up to 35 slices over a defocus range of −500 to −1200 Å. The bright spots composing a network of 3^6+3^2434 (1:6), 3^6+3^2434 (1:10) or $3^6+3^34^2$ (1:2) in the simulated image for the *F*, *K* or *J* phase can be obtained over a thickness range of 36 to 90, 36 to 67 or 23 to 158 Å at defocus values of −500, −673 or −950 Å, respectively. One of these series, namely those of the *F* phase, is shown in Fig. 1. Though the network of bright spots only shows the arrangement of the hexagonal antiprisms, it is sufficient to demonstrate the structural characteristics of the σ, *F*, *K* and *J* phases.

In our experimental images, the half-width of a Gaussian spread of defocus, the semi-angle of convergence and the size of the objective aperture were all kept at the same conditions and can be measured experimentally. The main factors affecting the image are the crystal thickness and defocus values. According to the results of image simulation, a good high-resolution image can be obtained either in the thinner side of the *Pendellösung* dark band at the Scherzer defocus (−673 Å) or in the thicker side of the first *Pendellösung* fringe at a defocus value of −950 Å. In both cases the hexagonal antiprisms were resolved as bright spots. Fig. 2 shows a general view of the *F* phase coexisting with the σ phase. In this high-resolution image these bright spots form nets of squares (4)

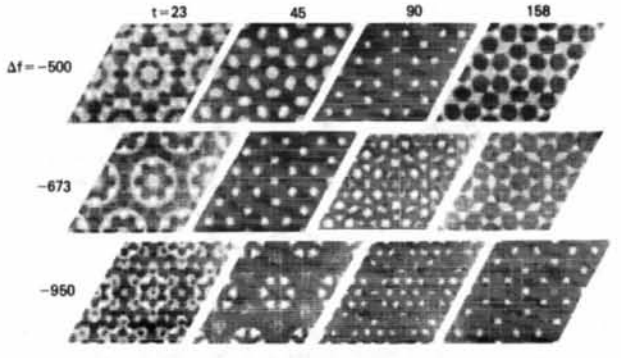

Fig. 1. Simulated [001] images of the *F* phase over a thickness range of 23 to 158 Å at defocus values of −500, −673 and −950 Å, respectively.

Table 1. *Parameters used for image simulation*

Electron wavelength (Å)	$2·507\times10^{-2}$
Spherical-aberration coefficient (mm)	1·2
Incident-beam divergence (rad)	$0·75\times10^{-3}$
Half-width of defocus spread due to chromatic aberration (Å)	70
Objective aperture ($Å^{-1}$)	0·55
Crystal thickness for one slice (Å)	4·5
Number of diffracted beams included in the dynamical diffraction calculation	1024

and triangles (3) and have a configuration of 3^2434 in σ and 3^6+3^2434 (1:6) in *F*. The distance between two bright spots in the image of the *F* phase is approximately 4·5 Å, being the same as in the σ phase. The match between these two phases is perfect and one zigzag sheet of bright spots (indicated by an arrow in Fig. 2) is common to both σ and *F* phases. Obviously, it is reasonable to suppose that the bright spots in the image of the *F* phase correspond also to the hexagonal antiprisms. In order to define the arrangement of the hexagonal antiprisms in the *F* phase, it is necessary to examine the arrangement of hexagonal antiprisms in the σ and *F* phases in high-resolution images (see Fig. 2). In both these phases, four hexagonal antiprisms form a square Cr_3Si unit (see Fig. 3). The atomic arrangement in the σ phase projected along [001] can be described as consisting of four square units (rotated 60 or 120° from each other) sharing corners, thus generating one unit of Zr_4Al_3 inside them (Fig. 3*a*). In the *F* phase, however, six square units of Cr_3Si rotated 60° from each other are joined by corner sharing, forming a hexagon

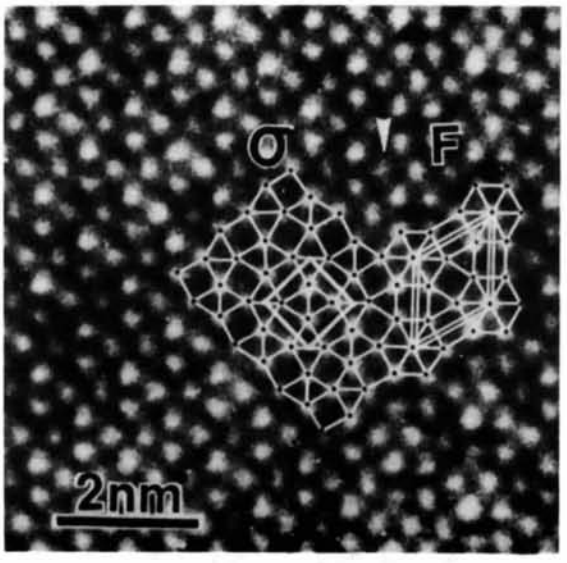

Fig. 2. A general view of the *F* phase coexisting with σ. The unit cells of σ and *F* are outlined by double lines. Networks of 3^2434 and 3^6+3^2434 of the σ and *F* phases, respectively, are also outlined. The match between these two phases (marked by an arrow) is perfect. (2 nm = 20 Å.)

Table 2. *Crystallographic data of the F phase*

$P6/mmm$; $a = b = 12{\cdot}5$, $c = 4{\cdot}5$ Å, $\gamma = 120°$, $Z = 52$.

Number	Position	Coordination number	Coordinates x	y	z
2	2(*d*)	15	$\frac{1}{3}$	$\frac{2}{3}$	$\frac{1}{4}$
2	2(*e*)	14	0	0	$\frac{1}{4}$
6	6(j_1)	15	0·223	0	0
6	6(j_2)	14	0·444	0	0
6	6(*k*)	12	$\frac{1}{2}$	0	$\frac{1}{2}$
6	6(*l*)	12	0·390	0·780	0
6	6(m_1)	12	0·112	0·223	$\frac{1}{2}$
6	6(m_2)	14	0·444	0·888	$\frac{1}{2}$
12	12(*o*)	14	0·223	0·446	$\frac{1}{4}$

consisting of three Zr_4Al_3 units (see Fig. 3*b*). There is a sixfold axis perpendicular to the plane of projection through the center of the hexagonal antiprism. It is noteworthy that, in the [001] projection of the σ phase, the edges of the square Cr_3Si unit are parallel to the $\langle 140\rangle_\sigma$ directions. On the basis of this suggested structural relationship between the F and σ phases, it can be seen from Figs. 2 and 3 that:

$$[100]_F \| [1\bar{1}0]_\sigma \quad a_F = b_F = \sqrt{2}a_\sigma$$
$$[010]_F \| [140]_\sigma \quad c_F = c_\sigma$$
$$[001]_F \| [001]_\sigma \quad \alpha = \beta = 90°,\ \gamma = 120°.$$

The HREM image of the F phase (Fig. 4) exhibits sixfold rotation and *mm* symmetry. According to the crystallographic structure data of the σ phase (space group $P4_2/mnm$ with an m plane perpendicular to the c axis, $a = 8{\cdot}91$, $c = 4{\cdot}5$ Å), the space group of F could be inferred as $P6/mmm$, $a = b = 12{\cdot}5$, $c = 4{\cdot}5$ Å, $Z = 52$. This is the hypothetical structure proposed by Frank & Kasper (1959, Fig. 16) and found recently by Lin & Steeds (1986). All the atomic parameters and coordination numbers are inferred, as given in Table 2, from the arrangement of the hexagonal antiprisms and the supposed symmetry. Fig. 5 shows the projection of the F phase along the [001] direction. The atoms in the layers at $z = 0$ and $\frac{1}{2}$ are indicated by open and filled circles, respectively, forming hexagons and triangles. The stacking arrangement of these layers has the effect of placing the hexagons over each other antisymmetrically, thus forming hexagonal antiprisms with tunnels inside them. There are also atoms in these tunnels at $z = \frac{1}{4}$ and $\frac{3}{4}$, indicated by double circles, forming nets of squares and triangles. Although the atomic species in the F phase are determined by X-ray energy-dispersive analysis, the atomic species in each position still remain unknown.

Fig. 6(*a*) shows the [001] electron diffraction pattern of the F phase and Fig. 6(*b*) is the calculated pattern using the data given in Table 1 and the atom positions in Table 2. The positions and intensities of the *hk*0 spots are consistent with the sixfold axis and *mm* symmetry of the [001] projection of the F phase. The unit-cell parameters a and b measured from the electron diffraction pattern agree also with the data listed in Table 2. The outermost region of calculated

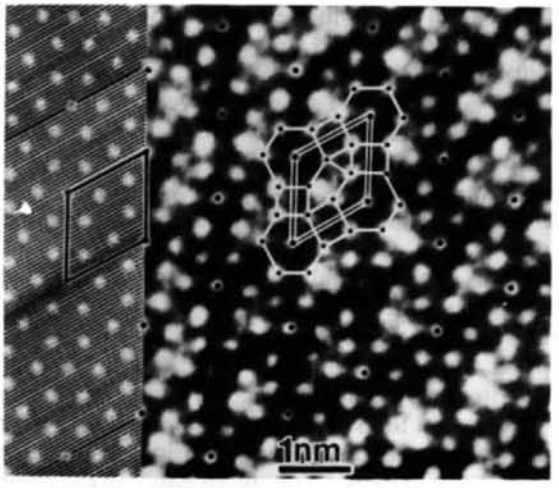

Fig. 4. [001] structural (right) and simulated (left) images of F. A bright spot corresponds to a hexagonal tunnel inside a column of hexagonal antiprisms. A unit cell is outlined. The simulated image was calculated at a defocus of −673 Å for a thickness of 68 Å.

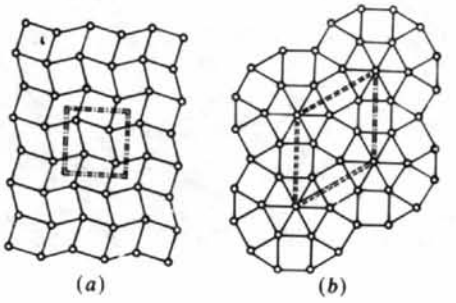

Fig. 3. 3^2434 and 3^6+3^2434 (1:6) networks of hexagonal antiprisms, represented by circles, in (*a*) σ and (*b*) F phases, respectively.

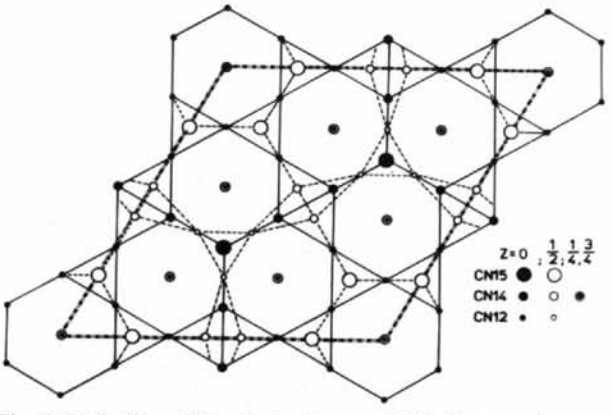

Fig. 5. Projection of the F structure on (001). Open circles are atoms at $z = 0$ and filled circles at $\frac{1}{2}$, forming hexagonal antiprisms with atoms inside them indicated by double circles at $\pm\frac{1}{4}$. The circles increase in size with coordinate number and a unit cell is outlined.

dynamical structure factors is 0·55 Å^{-1} in reciprocal space, corresponding to a maximum index of ±5 for $h00$ and $0k0$ reflections. Fig. 6(b) shows the calculated result for a thickness of 68 Å and the different sizes of the diffraction spots correspond to six grades of normalized calculated intensities. It should be noted that, according to calculation, the intensities of some diffracted beams are very weak or should disappear, but they appear, in fact, in the experimental diffraction pattern. This comes possibly from the variation of the thickness in a wedge-form crystal.

A simulated image of the F phase for a thickness of 68 Å at the Scherzer defocus, using the data given in Tables 1 and 2, is shown in Fig. 4 (left), which matches the observed one quite well. These confirm again a one-to-one correspondence between the bright spots in the high-resolution image and the hexagonal antiprisms in the structure of the F phase, possibly proving the correctness of the crystallographic data of the F phase.

Besides the F phase two more new phases, called K and J, have also been found in this Ni-based superalloy. Because these phases occur frequently in intimate intergrowth with the F phase in an aggregate of crystallites, the structure determination of K and J was greatly facilitated by the close relationship between them (see Figs. 13 and 14). The crystal structures of the K and J phases have also been determined by a similar procedure as above. For brevity, only the results of the analysis will be reported in the following. Fig. 7 (left) shows the structure image of the K phase, in which the bright spots form a net of squares (4) and triangles (3) with a configuration of 3^6+3^2434 (1:10). Fig. 8 is the [001] projection of the K-phase structure, which was inferred from the structure image of the K phase and the close structure relationship between the F and K phases. According to the relationship between the structures of σ and K it can be seen from Figs. 7 and 8 that:

$$[001]_K \| [1\bar{1}0]_\sigma \quad a_K = \sqrt{2}a_\sigma$$
$$[010]_K \| [110]_\sigma \quad b_K = 2a_\sigma \cos 14{\cdot}03°$$
$$[001]_K \| [001]_\sigma \quad c_K = c_\sigma$$
$$\alpha = \beta = \gamma = 90°,$$

where 14·03° is the angle between $[100]_\sigma$ and $[410]_\sigma$. The space group, unit-cell parameters and atomic coordinates are given in Table 3. Fig. 9(a) shows the [001] electron diffraction pattern of the K phase. In this pattern, some additional diffraction spots appeared and the intensity of the twelve stronger spots on the second circle is higher than that of the spots on the first circle. For example, the intensity of the 600 spot is higher than that of the 230 (see Fig. 9a), *etc.* This arises, perhaps, from the misalignment and curvature of the minute crystallite. However, it is very hard to obtain such an electron diffraction pattern of the K phase alone. Fig. 9(b) shows the normalized intensities of $hk0$ reflections of the K phase in six grades, calculated from the atomic positions given in Table 3 for a thickness of 68 Å. The hexagonal distribution of strong spots agrees with the experimental one, both being the result of juxtaposed hexagonal antiprisms (Ye, Wang & Kuo, 1985). The image simulation was carried out using the parameters given in Table 1 and the crystallographic data listed in Table 3. One of these simulated images is

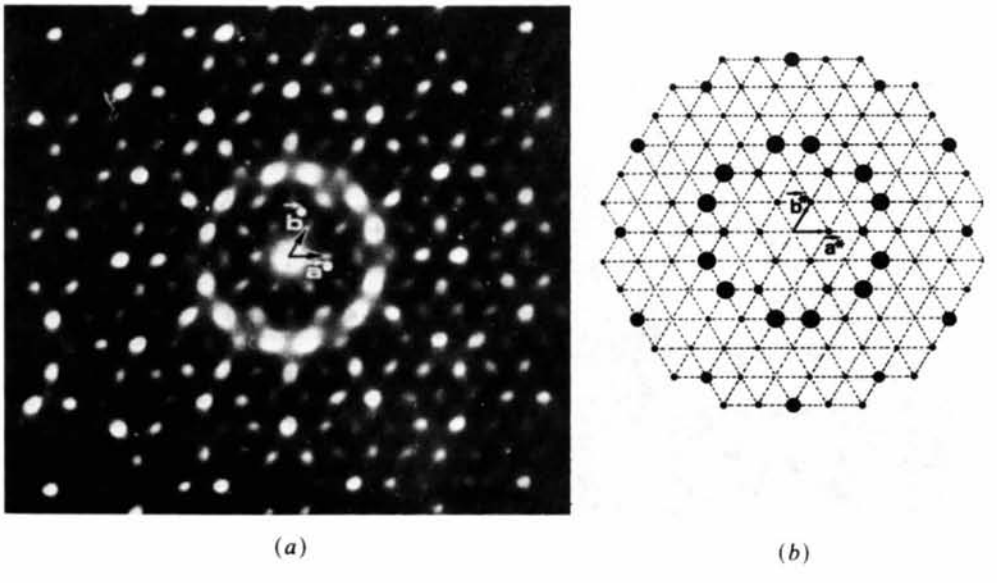

(a) (b)

Fig. 6. (a) A [001] electron diffraction pattern of the F phase. (b) Calculated [001] diffraction pattern. The size of the circle shows the relative intensity calculated from the structure of the F phase.

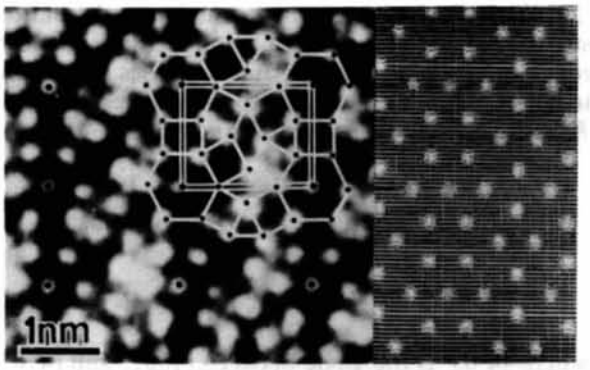

Fig. 7. [001] structural (left) and simulated (right) images of *K*. Bright spots correspond to hexagonal antiprisms of the *K* phase, forming a network of $3^6+3^24^34$ (1:10). A unit cell is outlined by double lines. The simulated image (right) was calculated at a defocus of −673 Å for a thickness of 68 Å, using the data given in Tables 1 and 3.

Table 3. *Crystallographic data of the K phase*

Pmmm; $a = 12{\cdot}5$, $b = 17{\cdot}1$, $c = 4{\cdot}5$ Å, $Z = 82$.

Number	Position	Coordination number	Coordinates x	y	z
1	1(*e*)	12	0	½	0
1	1(*h*)	12	½	½	½
2	2(i_1)	15	0·220	0	0
2	2(i_2)	14	0·442	0	0
2	2(*j*)	12	½	0	½
2	2(*k*)	15	0·392	½	0
2	2(n_1)	12	0	0·143	½
2	2(n_2)	15	0	0·430	½
2	2(*o*)	12	½	0·143	0
2	2(p_1)	14	½	0·072	½
2	2(p_2)	15	½	0·216	½
2	2(*q*)	14	0	0	½
4	4(*u*)	14	0	0·286	½
4	4(*v*)	14	½	0·358	½
4	4(*x*)	14	0·167	½	½
4	4(y_1)	12	0·085	0·376	0
4	4(y_2)	15	0·110	0·143	0
4	4(y_3)	14	0·220	0·286	0
4	4(y_4)	14	0·277	0·358	0
4	4(y_5)	12	0·415	0·253	0
4	4(z_1)	12	0·167	0·072	½
4	4(z_2)	12	0·167	0·216	½
4	4(z_3)	14	0·167	0·358	½
4	4(z_4)	14	½	0·286	½
4	4(x_5)	12	½	0·428	½
8	8(α)	14	½	0·143	½

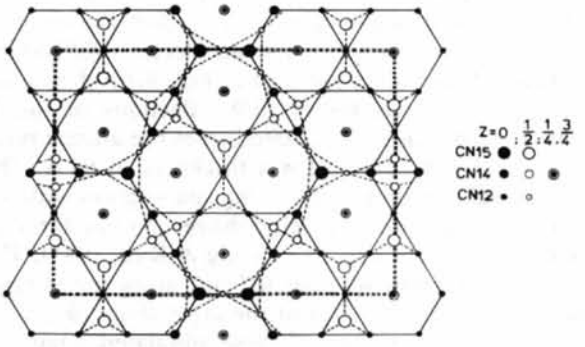

Fig. 8. A [001] projection of the *K* structure in which a unit cell is outlined by double dotted lines.

given in Fig. 7 (right) and it matches the observed one quite well, possibly confirming the correctness of the structure of the *K* phase.

The crystal structure of the *J* phase coexisting with *F* has been determined by the same method. Fig. 10 shows its structural and simulated images showing a good match between them. The bright spots in these images form a network of $3^6+3^34^2$ (1:2). The crystallographic data for the *J* phase derived from the high-resolution image are presented in Table 4. The [001] projection of the *J*-phase structure is shown in Fig. 11 and the structural relationship between the *J*

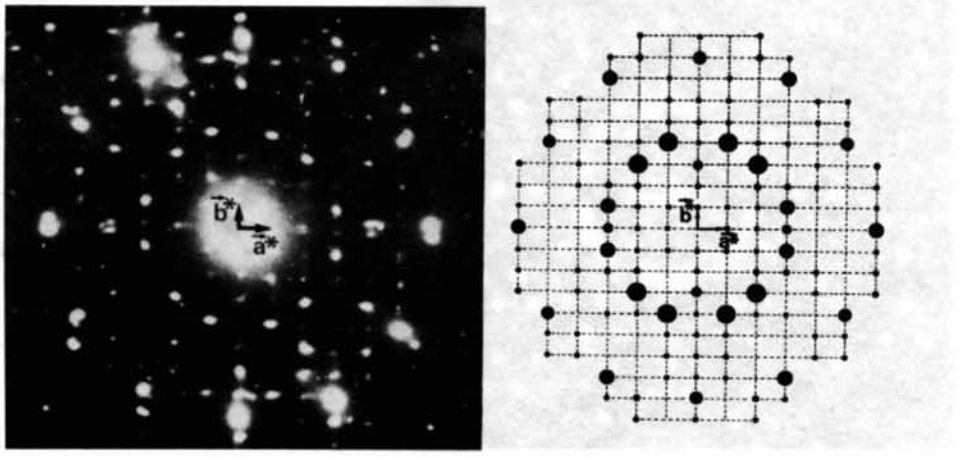

(*a*) (*b*)

Fig. 9. (*a*) A [001] electron diffraction pattern of the *K* phase. (*b*) Calculated [001] diffraction pattern. The size of the circle shows the relative intensity calculated from the structure of the *K* phase.

and σ phases is:

$$[100]_J \| [410]_\sigma \quad a_J = a_\sigma/2 \cos 14{\cdot}03°$$

$$[010]_J \| [\bar{1}40]_\sigma \quad b_J = a_\sigma \cos 14{\cdot}03° + a_\sigma \sin 14{\cdot}03° \,.\, c \operatorname{tg} 28{\cdot}06°$$

$$[001]_J \| [001]_\sigma \quad c_J = c_\sigma$$

$$\alpha = \beta = \gamma = 90°.$$

3. Discussion

These new phases, *F*, *K* and *J*, have been found, together with σ and *H*, in precipitates electrolytically extracted from a Ni-based superalloy. Since the perfect region of the crystallites is in general limited to a few thousand Å it is impossible to determine their structures by X-ray diffraction analysis. However, the crystal structures of these new phases, thanks to their close relations to the σ phase, can still be determined by high-resolution electron microscopy combined with image simulation and selected-area electron diffraction.

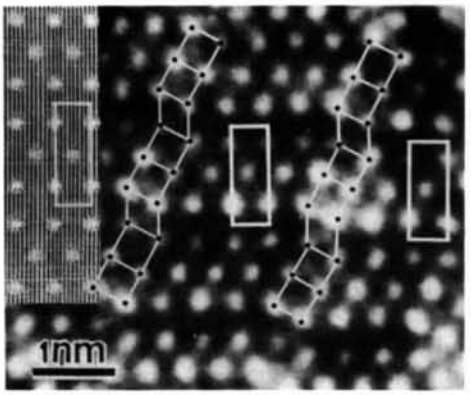

Fig. 10. [001] structural and simulated (upper left) images of the *J* phase. Bright spots correspond to hexagonal antiprisms of the *J* phase forming a network of $3^6+3^34^2$ (1:2). Unit cells are outlined. The simulated image was calculated at a defocus of −673 Å for a thickness of 68 Å, which matches the structure image quite well.

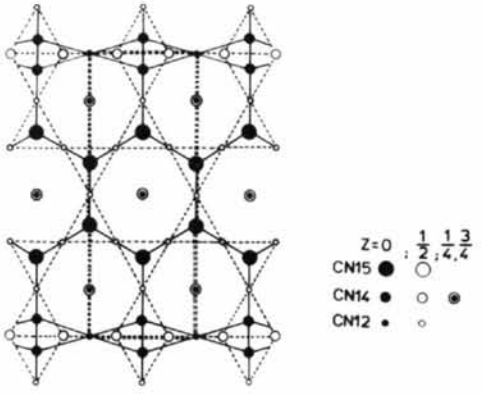

Fig. 11. A [001] projection of the structure of the *J* phase. A unit cell is outlined by double dotted lines.

Table 4. *Crystallographic data of the J phase*

Pmmm; $a = 4{\cdot}5$, $b = 12{\cdot}5$, $c = 4{\cdot}5$ Å, $Z = 22$.

Number	Position	Coordination number	Coordinates x	y	z
1	1(*a*)	12	0	0	0
1	1(*g*)	12	0	$\frac{1}{2}$	$\frac{1}{2}$
2	2(*j*)	14	0·259	0	$\frac{1}{2}$
2	2(*m*)	15	0	0·387	0
2	2(o_1)	14	$\frac{1}{2}$	0·060	0
2	2(o_2)	15	$\frac{1}{2}$	0·280	0
2	2(*p*)	12	$\frac{1}{2}$	0·167	$\frac{1}{4}$
2	2(*t*)	14	$\frac{1}{2}$	$\frac{1}{2}$	$\frac{1}{4}$
4	4(*u*)	14	0	0·167	$\frac{1}{4}$
4	4(*z*)	12	0·259	$\frac{1}{2}$	$\frac{1}{2}$

Several research groups have studied the structure description of the tetrahedrally close-packed phases (Frank & Kasper, 1959; Shoemaker & Shoemaker, 1969; Andersson, 1978). It has been pointed out by Andersson (1978) that all these complex structures of tetrahedrally close-packed phases can be derived from such relatively simple structures as Cr_3Si and Zr_4Al_3 with 4^4 and 3^6 nets of hexagonal antiprisms by such crystallographic operations as translation, rotation, reflection, chemical twinning and intergrowth. According to the viewpoint of this building principle, the σ phase can be generated from the Zr_4Al_3 and Cr_3Si structural units in 3^24^34 juxtaposition. The intergrowth of the Zr_4Al_3 and Cr_3Si structural units can also form the *H* structure with a 3^34^2 net (Ye, Li & Kuo, 1984). These new complex structures, such as *F*, *K* and *J*, can also be built from these building blocks by suitable crystallographic

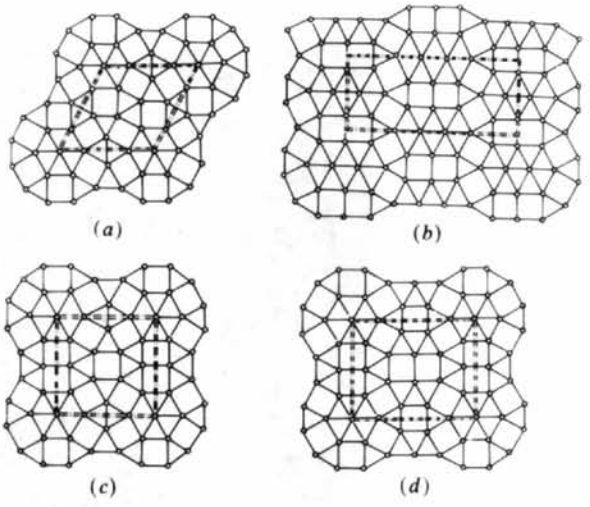

Fig. 12. Schematic diagram of the hypothetical structures. Hexagonal antiprisms represented by open circles forming networks of $3^6+3^24^34$ (1:12), $3^6+3^34^2+3^24^34$ (1:1:3), $3^6+3^34^2+3^24^34$ (1:2:12) and $3^6+3^34^2+3^24^34$ (1:4:14) for (*a*) Hy-1, (*b*) Hy-2, (*c*) Hy-3 and (*d*) Hy-4, respectively.

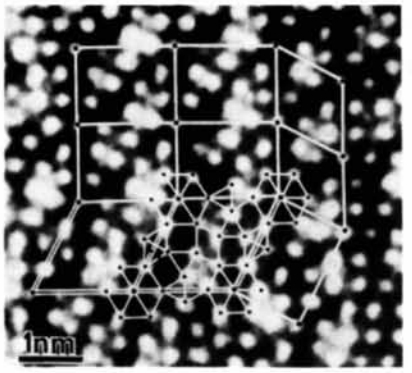

(*a*)

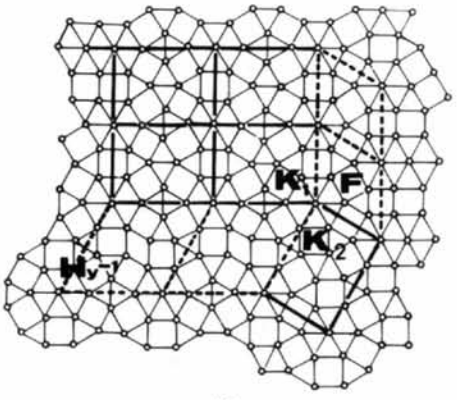

(*b*)

Fig. 13. (*a*) The structure of the rotation domains of the *K* phase coexisting with *F* and a hypothetical structure, called Hy-1, appearing between these domains. The unit cell of the Hy-1 structure is outlined by double lines. (*b*) Corresponding structure model showing the network of hexagonal antiprisms.

Table 5. *Crystal structure of σ-related phases*

Phase	Space group	Network of the second layers	Lattice constants (Å) a_0	b_0	c_0	Atoms per unit cell
σ	$P4_2/mnm$	3^2434	8·8		4·5	30
H	*Cmmm*	3^34^2	4·5	17·5	4·5	30
F	*P6/mmm*	3^6+3^2434 (1:6)	12·5	12·5	4·5	52
K	*Pmmm*	3^6+3^2434 (1:10)	12·5	17·1	4·5	82
J	*Pmmm*	$3^6+3^34^2$ (1:2)	4·5	12·5	4·5	22
Hypothetical structures						
Hy-1	*P6/mmm*	3^6+3^2434 (1:12)	17·1	17·1	4·5	97
Hy-2	*Cmmm*	$3^6+3^34^2+3^2434$ (1:1:3)	12·5	31·0	4·5	148
Hy-3	*Pmmm*	$3^6+3^34^2+3^2434$ (1:2:12)	17·1	17·1	4·5	112
Hy-4	*Pmmm*	$3^6+3^34^2+3^2434$ (1:4:14)	17·1	21·7	4·5	142

operations (see Table 5). Moreover, some more hypothetical structures listed in Table 5 can be derived without changing either the coordination number or the distance of neighboring atoms. Fig. 12 is a schematic diagram of four hypothetical σ-related structures which are also built from Zr_4Al_3 and Cr_3Si blocks in different configurations forming respectively 3^6+3^2434 (1:12), $3^6+3^34^2+3^2434$ (1:1:3), $3^6+3^34^2+3^2434$ (1:2:12) and $3^6+3^34^2+3^2434$ (1:4:14) networks of hexagonal antiprisms. Though no diffraction pattern of these hypothetical structures has been obtained, small regions of these structures can easily be identified in the high-resolution electron micrograph. Fig. 13 shows two rotation domains of the *K* phase and the domain of a new hypothetical structure, called Hy-1, between them. Fig. 14 shows two rotation domains of the *J* phase and in one of these there are parallel domains separated by a boundary along (110), indicated by arrows. Between J_1 and J_2 a wedge of *F* and *K* structures occurred. Since all these struc-

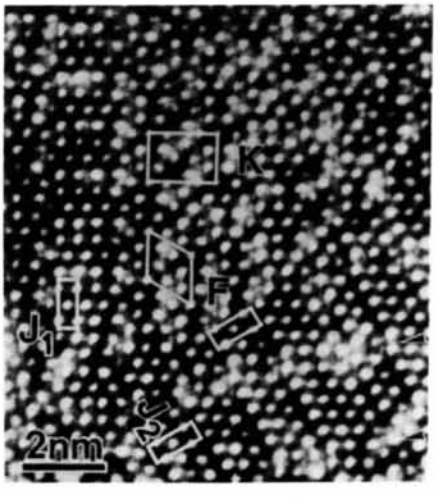

(*a*)

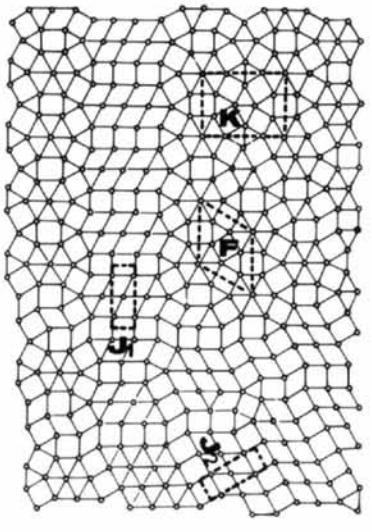

(*b*)

Fig. 14. (*a*) Structural image of the parallel and rotation domains of the *J* phase with the *F* and *K* structures occurring between them, and (*b*) the corresponding structure model showing the arrangement of hexagonal antiprisms.

tures are composed of the same Zr_4Al_3 and Cr_3Si building blocks, they can intergrow easily and the match between these domains is therefore generally good.

The authors would like to thank Drs Y. D. Lin and J. W. Steeds of Bristol University for providing unpublished structural information of a new phase identical to our *F* phase. Throughout this work we have enjoyed many stimulating discussions with Professor H. Q. Ye of our laboratory.

References

ANDERSSON, S. (1978). *J. Solid State Chem.* **23**, 191-204.
FRANK, F. C. & KASPER, J. S. (1959). *Acta Cryst.* **12**, 483-499.
ISHIZUKA, K. (1982). *Acta Cryst.* A**38**, 773-779.
LIN, Y. P. & STEEDS, J. W. (1986). *Acta Cryst.* B**42**, 159-162.
SHOEMAKER, C. B. & SHOEMAKER, D. P. (1969). *Developments in the Structural Chemistry of Alloy Phases*, pp. 107-139. New York: Plenum.
YE, H. Q. & KUO, K. H. (1984). *Philos. Mag.* A**50**, 117-132.
YE, H. Q., LI, D. X. & KUO, K. H. (1984). *Acta Cryst.* B**40**, 461-465.
YE, H. Q., WANG, D. N. & KUO, K. H. (1985). *Ultramicroscopy*, **16**, 273-278.

Acta Cryst. (1986). B**42**, 159-162

Identification of a Hitherto Unreported Frank–Kasper Phase

BY Y. P. LIN AND J. W. STEEDS

H. H. Wills Physics Laboratory, Tyndall Avenue, Bristol BS8 1TL, England

(*Received* 1 *March* 1985; *accepted* 20 *December* 1985)

Abstract

A previously unreported intermetallic phase has been discovered in a commercial superalloy. The phase was generally found in a highly faulted state. Small regular regions have been investigated by convergent-beam electron diffraction to give a space group of $P6/mmm$ and cell constants $a_0 = 12{\cdot}6 \pm 0{\cdot}1$ and $c_0 = 4{\cdot}6 \pm 0{\cdot}05$ Å. The diffracted intensities and some preliminary high-resolution micrographs indicate that the phase is one of those proposed by Frank & Kasper [*Acta Cryst.* (1959), **12**, 483-499], but not previously observed. Parallel work in China on another alloy has identified an apparently similar phase, named *F* phase, a description adopted here.

Introduction

Many intermetallic compounds, particularly those formed by transition metals, can be classified as having tetrahedrally close-packed structures containing interpenetrating polyhedra with coordination numbers 12, 14, 15 or 16 (Frank & Kasper 1958, 1959; Shoemaker & Shoemaker, 1969). Frank & Kasper showed that most of these compounds are layer-structured and that whole families of structures, including some hypothetical ones, could be generated by stacking similar layers in different ways and by introducing tessellation faults. The structure of these compounds generally consists of two primary layers at $z = 0$ and $\frac{1}{2}$ formed by tessellations of triangles and either hexagons or pentagons. Two identical secondary layers, at $z = \frac{1}{4}$ and $\frac{3}{4}$, centre the hexagonal or pentagonal antiprisms formed by the superposition of the primary layers.

We report here the space group of an intermetallic phase with a structure apparently agreeing with one predicted by Frank & Kasper (1959) in which the primary layers consist of a tessellation of hexagons and triangles, while the secondary layers consist of a $3^6 + 3^2\,434$ (1:6) net (for notation, see Pearson, 1972). The new phase has been named *F* in honour of the work of Frank & Kasper at the suggestion of Professor Kuo, who has, with Dr Li, simultaneously and independently identified the phase using high-resolution electron microscopy (Li & Kuo, 1986).

Experimental

The new phase was found in a Ni-based powder-metallurgical superalloy with the following composition (in wt%): Cr 10·0, Co 15·0, W 6·0, Mo 3·0, Ti 4·0, Al 4·0, Nb 1·7, Hf 0·7, Fe < 1·0, Mn < 0·15, Si < 0·2, Zr 0·05, C 0·04, B 0·002, Ni balance (these values were obtained from the suppliers: Rolls Royce Ltd, Filton, England.)

After hot isostatic pressing at 1443 K, the alloy was forged at 1423 K, solution treated at 1450 K for 4 h and aged at 1033 K for 16 h. Carbon-extraction replicas were prepared from gauge sections of samples which had been either creep tested at 953 K

0108-7681/86/020159-04$01.50